Influence of initial film radius and film thickness on the rupture of foam films

Shah, Maulik S.; Kleijn, Chris R.; Kreutzer, Michiel T.; Van Steijn, Volkert

DOI
10.1103/PhysRevFluids.6.013603

Publication date
2021

Document Version
Final published version

Published in
Physical Review Fluids

Influence of initial film radius and film thickness on the rupture of foam films

Maulik S. Shah, Chris R. Kleijn, Michiel T. Kreutzer, and Volkert van Steijn*
Department of Chemical Engineering, Delft University of Technology van der Maasweg 9, 2629 HZ, Delft, The Netherlands

(Received 30 April 2020; accepted 24 November 2020; published 11 January 2021)

The initial thickness and radius of the film that forms upon close contact of two foam bubbles are known to influence the thinning dynamics and lifetime of the film. Various scalings of lifetime t_r, with initial radius R_{film} and thickness h_o, have been proposed in literature. In this paper, we present a hydrodynamic thin-film model that includes both surface tension, van der Waals forces, and drainage and that clarifies the various proposed scalings of lifetime. Our model equations were solved numerically for a range of R_{film} and h_o as direct input parameters. Films with a large radius are found to thin locally at a dimple, while films with a small radius thin across the entire film. The observed dynamics and lifetime were interpreted by developing a simplified model that describes the early stage dimpled drainage and the late stage van der Waals thinning, using known similarity solutions. For large radii films, our simulations confirm earlier theoretical work on semi-infinite films that predicts $t_r \sim R_{\text{film}}^0 h_0^{5/7}$. For small radii films, our numerical simulations show the opposite trend with lifetime being solely dependent on R_{film}, in fair agreement with the simplified model that predicts $t_r \sim R_{\text{film}}^{10/7} h_0^0$.

DOI: 10.1103/PhysRevFluids.6.013603

I. INTRODUCTION

The stability of foams and emulsions is largely determined by the lifetime of the thin liquid film that forms between two bubbles or droplets upon close contact. Thinning of this film is mediated by drainage induced by the pressure difference between the film and the Plateau border. Once the film gets thinner than $O(100\ \text{nm})$, destabilizing van der Waals forces overtake the thinning process and induce rupture of the film. Together, the early stage drainage and late stage rupture, which partially overlap, determine the lifetime of the film.

Classical theory by Reynolds [1] describes the thinning of the film between the two bubbles by considering a fluid between two plane-parallel rigid disks subjected to drainage. It teaches that the approaching velocity of the discs is constant in time and depends on the imposed suction pressure and disk radius. Vrij [2] extended Reynolds' theory by postulating that the film thins uniformly with the velocity predicted by Reynolds' theory only down to a critical thickness. This critical thickness marks the neutral stability of waves on the film due to the interplay between stabilizing surface tension forces and destabilizing van der Waals forces. Upon further thinning, these waves, which originate from thermal fluctuations, exhibit an exponential growth that outruns the Reynolds' velocity, perturbing the interface until rupture occurs randomly at one of the troughs on the surface of the film. However, earliest experiments in so-called Scheludko cells are at odds with this picture: instead of uniform initial thinning, a local depression immediately develops near the Plateau border, and this so-called "dimple" thins out more rapidly than the central part of the film [3–5]. The formation of a dimple was first studied theoretically by Frankel and Mysels [6], who developed scaling rules for film thinning at the center and at the periphery of the film. A criterion that describes

*v.vansteijn@tudelft.nl

whether and when a film primarily thins uniformly or locally through a dimple was developed by Joye *et al.* [7] and Singh *et al.* [8] based on a comparison between the curvature in the dimple and in the Plateau border. For many practical systems, this geometric criterion teaches us that films with a radius larger than about 50 μm develop dimples in the film-thinning process. Taken altogether, the film-thinning process comprises of an early drainage stage, that has been found to proceed via the formation of a dimple, and a late rupture stage, where destabilizing van der Waals forces induce rupture that may be enhanced through the amplification of perturbations on the interface.

A well-established theoretical description of film thinning is rooted in the thin-film equation, which has been shown to accurately describe spatiotemporal profiles of the film and its lifetime as reported for controlled drainage experiments between two bubbles or two droplets [9–12] and between a bubble or droplet and a solid substrate [13–17]. Being a fourth-order nonlinear partial differential equation, it is commonly solved numerically. An important aspect to be considered is how to incorporate the approach of two initially spherical bubbles, and the resulting shape of the thin film that subsequently forms between the flattened bubbles [18–20], into the thin-film description. More specifically, the extent over which the film is flattened, referred to as the film radius, has been shown to depend on the approach velocity in Atomic Force Microscopy (AFM) measurements [19] and on the rate at which liquid is withdrawn between two bubbles in Scheludko cell experiments [7,18]. A common way to incorporate these effects in the thin-film description is to introduce an external force that drives the initially spherical interfaces together, which is switched off once a flattened film has formed in order to study the thinning dynamics in the absence of this external force [9]. In order to single out the effect of the initial features of the flattened film, i.e., its radius and its thickness, we developed a simplified description that allows to immediately start from a flattened film with prespecified radius and thickness. We use this approach to resolve the debated question as to how initial film radius and thickness influence thinning dynamics and film lifetime. This debate stems from the various simplifications to the classical thin-film equation that have been used to answer the question using analytical techniques.

Assuming the film to be planar and to thin quasistatistically, Reynolds' theory and later refinements to the same analytically predict the lifetime to scale with film radius as $t_r \sim R_{\text{film}}^2$ [1,21]. Relaxing the quasisteady assumption to include the influence of drainage on the growth of waves in a plane-parallel film, and using experimentally observed thinning rates, Sharma and Ruckenstein [22] predicted $t_r \sim R_{\text{film}}^1$. Malhotra and Wasan [23] performed numerical simulations using the thin-film equation that solved exclusively for the flow in the Plateau border, while assuming that the film remains essentially plane parallel, to find $t_r \sim R_{\text{film}}^{4/5}$. Although this model is in reasonable agreement with experimentally observed lifetimes, photographic techniques have shown that draining films are not plane parallel [5,24,25]. This finding inspired the development of several theories that either take into account quasistationary nonhomogeneities on a plane-parallel interface resulting in $t_r \sim R_{\text{film}}^{4/5}$ (commonly referred as the after Manev, Tsekov, and Radoev (MTR) theory) [24–26], or assume the translatory and oscillatory motion of hydrodynamic waves on a plane-parallel interface resulting in $t_r \sim R_{\text{film}}^{3/4}$ [27]. With the inclusion of the aforementioned nonhomogeneities, these theories address the notion that film thinning is not strictly plane parallel in nature. However, they fail to capture the pronounced dimple shapes observed in the experiments [5,11,12,28]. Aside from the development of steady and nonsteady plane-parallel models, with and without nonhomogeneities, models have been developed on quasisteady nonplanar films featuring dimples. With the interface shape no longer fixed, but freely deformable, an analysis of the spatiotemporal film profiles is significantly simplified when assuming that the flow at the periphery of the film is independent of its radial location. Using such a quasisteady approach, Frankel and Mysels [6] calculated the shape of a dimple close to rupture. Aradian *et al.* [29] developed a comprehensive model for dimpling (referred as marginal pinching in their work) that extended the model of Frankel and Mysels [6] for infinitely large films. However, both of these works do not include van der Waals forces. Without their inclusion, films do not rupture (i.e., reach a zero thickness asymptotically) such that the lifetime of the film and its dependency on film radius and thickness cannot be predicted by these models.

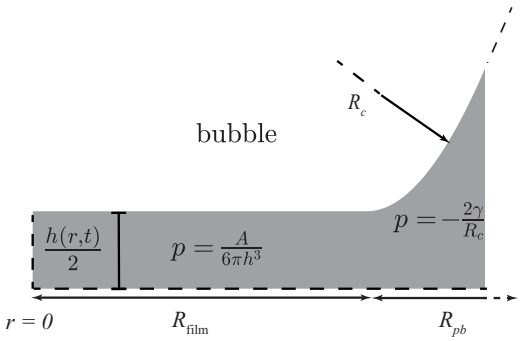

FIG. 1. Schematic of an axisymmetric nonplanar thin liquid film between two gas bubbles with the film thickness parameterized by $h(r, t)$. Since the geometry is mirror symmetric, we here display the upper half. The initial film shows a flat part extending from $0 < r \leqslant R_{\text{film}}$ with the pressure primarily given by the van der Waals component of the disjoining pressure $p \sim A/6\pi h^3$. This flat part is connected to a curved part extending from $R_{\text{film}} < r \leqslant R_{\text{film}} + R_{pb}$ with the pressure primarily given by the Laplace pressure $p \sim -2\gamma/R_c$, with $2/R_c$ as the curvature imposed at the edge. The dashed line at $r = 0$ signifies the second symmetry of the problem, viz., the axisymmetry in the system.

In this work, we clarify the variety of scaling rules in the literature, stemming from various applied simplifications, by numerically solving the thin-film equation without such simplifications, using initial film radius and thickness as direct input parameters. To mechanistically explain the numerically obtained dependency of the lifetime of the film on its initial radius and thickness, we combined earlier-reported analytical models for dimpling in the early stage [6] and rupture through van der Waals forces in the late stage [30]. While these models were obtained through simplification of the full thin-film equation, the combined model presented here does corroborate the dependency found in our simulations of the full thin-film equation.

II. PROBLEM FORMULATION

We study the evolution of an axisymmetric nonplanar thin liquid film with viscosity μ and surface tension γ between two gas bubbles. The spatiotemporal thickness of the film is parameterized by $h(r, t)$. Since the geometry of the problem is mirror symmetric, we consider only one half of the film as shown in Fig. 1. Throughout this work, the term "thickness" is used to refer to the full film thickness $h(r, t)$. The film comprises of a flat part between $0 < r \leqslant R_{\text{film}}$ of initial thickness h_o, connected to a curved part between $R_{\text{film}} \leqslant r \leqslant R_{\text{film}} + R_{pb}$, with a curvature $2/R_c$ corresponding to a Plateau border. Considering the pressure in the gas phase to be uniform and setting it equal to zero, the pressure p in the curved part of the liquid film, where intermolecular forces play an insignificant role, is dictated primarily by the Laplace pressure and of order $p = -2\gamma/R_c$. Conversely, the pressure in the thin flat part is dictated by intermolecular forces, which in this paper are considered as attractive van der Waals forces, such that it is of order $p = A/6\pi h^3$, with A being the Hamaker constant. The difference in pressure drains the liquid from the flatter part of the film to the more curved part.

The axisymmetric thin-film equation that describes the evolution of nonplanar thin films can be derived by applying a long-wave approximation to the incompressible Navier-Stokes equations [31,32]. We consider rigid interfaces which could be encountered in surfactant-rich systems or even in systems with traces of impurities. These interfaces are described by commonly encountered tangentially immobile boundary conditions [19], which then yields

$$\frac{\partial h}{\partial t} = \frac{1}{12\mu}\frac{1}{r}\frac{\partial}{\partial r}\left\{rh^3\frac{\partial}{\partial r}\left[\frac{A}{6\pi h^3} - \frac{\gamma}{2r}\frac{\partial}{\partial r}\left(r\frac{\partial h}{\partial r}\right)\right]\right\}, \tag{1}$$

with the first term on the right side arising from long-ranged attractive van der Waals forces and the second term from surface tension forces. Since the problem we consider is axisymmetric around $r = 0$, at the left boundary of our domain, gradients in thickness and pressure are zero, i.e.,

$$\frac{\partial h}{\partial r} = 0, \quad \frac{\partial p}{\partial r} = 0, \quad \text{both at } (r = 0). \tag{2}$$

Using $p = A/6\pi h^3 - \gamma/2r(\partial/\partial r(r\partial h/\partial r))$, the boundary condition for pressure becomes $\frac{A}{2\pi h^4}\frac{\partial h}{\partial r} + \frac{\gamma}{2}\frac{\partial}{\partial r}(\frac{1}{r}\frac{\partial h}{\partial r} + \frac{\partial^2 h}{\partial r^2}) = 0$ at $r = 0$, which simplifies to $\partial^3 h/\partial r^3(r = 0) = 0$ when using the first boundary condition $\partial h/\partial r(r = 0) = 0$ together with the notion that the two principal curvatures are the same at $r = 0$ due to axisymmetry. A Plateau border of constant curvature is obtained by imposing its shape, i.e., curvature $(2/R_c)$[1] and corresponding height, at the other domain boundary $(r = R_{\text{film}} + R_{pb})$, i.e.,

$$\left.\begin{aligned} \frac{1}{2r}\frac{\partial}{\partial r}\left(r\frac{\partial h}{\partial r}\right) &= \frac{2}{R_c}, \quad \text{at } (r = R_{\text{film}} + R_{pb}) \\ h = h_o + \frac{(r^2 - R_{\text{film}}^2)}{R_c} &+ \frac{2R_{\text{film}}^2}{R_c}\ln\left(\frac{R_{\text{film}}}{r}\right), \quad \text{at } (r = R_{\text{film}} + R_{pb}) \end{aligned}\right\}. \tag{3}$$

This height is obtained by integrating the expression for constant curvature in the curved meniscus and imposing that the height and its first derivative match the planar part of the film at $r = R_{\text{film}}$, i.e., $h(r = R_{\text{film}}) = h_o$ and $\partial h/\partial r(r = R_{\text{film}}) = 0$.

The initial film profile is described by a flat film connected to a Plateau border of constant curvature, i.e.,

$$\left.\begin{aligned} h &= h_o, \quad \text{at } (0 < r \leqslant R_{\text{film}}, t = 0) \\ h = h_o + \frac{(r^2 - R_{\text{film}}^2)}{R_c} &+ \frac{2R_{\text{film}}^2}{R_c}\ln\left(\frac{R_{\text{film}}}{r}\right), \quad \text{at } (R_{\text{film}} < r \leqslant R_{\text{film}} + R_{pb}, t = 0) \end{aligned}\right\}. \tag{4}$$

While the height and its first derivative smoothly connect the flat and the curved parts, we note that the second derivative is discontinuous. Although the corresponding pressure profile is discontinuous at the connection, we confirm from checking the pressure profiles that this discontinuity equilibrates very quickly, i.e., in less than 0.01% of the lifetime. Additionally, eliminating the pressure discontinuity by using an initial condition that connects the flat part to the curved part using a transition region [33], we see that the resulting profiles (see Fig. 2) overlap those without the transition region soon after the start (for $t \gtrsim t_r/8$). Furthermore, the addition of a significant perturbation representative of hydrodynamic nonhomogeneities in the initial condition, as indicated by the red dashed curves in Fig. 2, also proves to be inconsequential in determining the lifetime and the film profile at the instant of rupture. This initial condition independency study ensures that the film dynamics during almost the entire process and the resulting lifetime are not affected by the choice of our initial condition.

The governing equation, boundary, and initial conditions are provided in dimensional form and show that the problem is governed by six parameters, which include three material properties, i.e., μ, γ, and A, and three geometric parameters, i.e., h_o, R_c, and R_{film}. The solution is insensitive to the chosen value of R_{pb} (see Fig. 1) as long as it lies between an upper and a lower bound. The upper bound is dictated by the validity of lubrication approximation, i.e.,

[1]In experiments, the radius of the capillary R_c directly governs the curvature of the interface and thereby the amount of capillary suction. In our numerical model, the capillary itself is not incorporated into the domain and we specify a constant curvature $2/R_c$, sufficiently far away from the flat part of the film such that the dynamics and lifetime are independent of the location of this boundary, such that R_{pb} does not play a role.

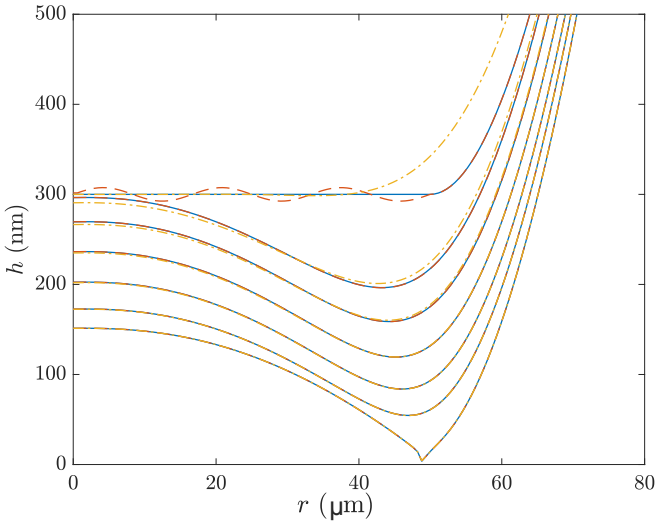

FIG. 2. Evolution of a film with initial thickness $h_o = 300$ nm and radius $R_{\text{film}} = 50\ \mu$m, with three different initial conditions. Blue solid lines correspond to the initial condition prescribed in Eq. (4). Red dashed lines correspond to an initial condition where a small sinusoidal perturbation with an amplitude of 25 nm and a wavelength of 16.7 μm is added to the flat part of the initial condition in Eq. (4). Yellow dashed-dotted lines correspond to a film that has a transition region from the flat portion of the film to the curved portion, with transition region as determined in Eq. (1) in the Supplemental Material. Aside from the initial profiles at $t = 0$, profiles are shown for $t_r/2^n$ with $n = 5, \ldots, 0$, with the rupture times t_r being 15.74, 15.74, and 15.69 s for these three initial conditions, respectively.

$R_{pb} \ll R_c/4(1 + \sqrt{(1 + 16R_{\text{film}}^2/R_c^2)}) - R_{\text{film}}$, while the lower bound is dictated by the region where curvature goes from practically zero in the flat part to $2/R_c$ in the curved part. This leads to $R_{pb} \gg \sqrt{h_o R_c}$, as discussed in more detail in Shah *et al.* [35].

We now perform a scaling analysis to demonstrate that the problem is governed by two dimensionless parameters. Using a height scale $h^* = h_o$, a radial scale $r^* = \sqrt{h_o R_c/4}$ [obtained from the constant curvature boundary condition at far right, i.e., Eq. (3)] and a timescale $t^* = 3\mu R_c^2/2\gamma h_o$, we obtain the dimensionless variables $\tilde{h} = h/h^*$, $\tilde{r} = r/r^*$, and $\tilde{t} = t/t^*$ together with the following dimensionless governing equation:

$$\frac{\partial \tilde{h}}{\partial \tilde{t}} = \frac{1}{\tilde{r}}\frac{\partial}{\partial \tilde{r}}\left\{\tilde{r}\tilde{h}^3\frac{\partial}{\partial \tilde{r}}\left[\frac{1}{12\kappa}\frac{1}{\tilde{h}^3} - \frac{1}{\tilde{r}}\frac{\partial}{\partial \tilde{r}}\left(\tilde{r}\frac{\partial \tilde{h}}{\partial \tilde{r}}\right)\right]\right\}, \tag{5}$$

where $\kappa = \pi h_o^3\gamma/AR_c$ is the relative strength of drainage. It signifies the ratio of the Laplace pressure and the initial van der Waals pressure. Additionally, we obtain the dimensionless boundary conditions

$$\left.\begin{aligned} \frac{\partial \tilde{h}}{\partial \tilde{r}} = 0,\ \frac{\partial^3 \tilde{h}}{\partial \tilde{r}^3} = 0, \quad &\text{both at } (\tilde{r} = 0) \\ \frac{1}{\tilde{r}}\frac{\partial}{\partial \tilde{r}}\left(\tilde{r}\frac{\partial \tilde{h}}{\partial \tilde{r}}\right) = 1, \quad &\text{at } (\tilde{r} = \tilde{R}_{\text{film}} + \tilde{R}_{pb}) \\ \tilde{h} = 1 + \frac{(\tilde{r}^2 - \tilde{R}_{\text{film}}^2)}{4} + \frac{\tilde{R}_{\text{film}}^2}{2}\ln\left(\frac{\tilde{R}_{\text{film}}}{\tilde{r}}\right), \quad &\text{at } (\tilde{r} = \tilde{R}_{\text{film}} + \tilde{R}_{pb}) \end{aligned}\right\} \tag{6}$$

and dimensionless initial condition

$$\left.\begin{aligned} \tilde{h} &= 1, \quad \text{at } (0 < \tilde{r} \leqslant \tilde{R}_{\text{film}}, \tilde{t} = 0) \\ \tilde{h} &= 1 + \frac{(\tilde{r}^2 - \tilde{R}_{\text{film}}^2)}{4} + \frac{\tilde{R}_{\text{film}}^2}{2} \ln\left(\frac{\tilde{R}_{\text{film}}}{\tilde{r}}\right), \quad \text{at } (\tilde{R}_{\text{film}} < \tilde{r} \leqslant \tilde{R}_{\text{film}} + \tilde{R}_{pb}, \tilde{t} = 0) \end{aligned}\right\} \tag{7}$$

with R_{film} and R_{pb} made dimensionless using r^*. With $\tilde{R}_{pb}$ chosen such that the solution is insensitive to its value, this scaling analysis shows that the problem is fully governed by two dimensionless control parameters, i.e., the relative strength of drainage κ and the film radius $\tilde{R}_{\text{film}}$.[2] We explore the parameter space by varying these two dimensionless parameters. As the main aim of this work is to understand how film dynamics depend on the initial features of the film, i.e., the film radius and its thickness, we translate the dimensionless representation back to the dimensional one. This is done by fixing μ, γ, A, and R_c, as is for example the case when performing experiments with a given set of working fluids in a capillary of given radius in a so-called Scheludko cell. Motivated by the experimental parameter range (using different fluids in a single capillary) from Manev *et al.* [25], we use $\mu = 0.000\,89$ Pa s, $\gamma = 0.0445$ N/m, $A = 1.5 \times 10^{-20}$ J, and $R_c = 1.8$ mm. The dimensional parameter space is then spanned by the initial film thickness h_0 from 300–2000 nm and the film radius R_{film} from 40–4000 μm. Note that in our simulations, we are able to control these parameters independently, while they are coupled in experiments through the flow rate at which liquid is withdrawn between two bubbles prior to the start of the film rupture experiments [7].

We conclude our problem formulation with a note on thermal fluctuations at the gas-liquid interface. These fluctuations do significantly influence film dynamics and rupture time in case of weak drainage ($\kappa \ll 1$), as shown in our previous work [18]. The focal point in this work is on cases with $\kappa \gg 1$, such that we have not included thermal fluctuations in our problem description. This is also further corroborated with the notion that films with a small radius are stable against waves because the unstable ones have wavelengths that exceed the radius of the film [9,19].

III. NUMERICAL IMPLEMENTATION

We numerically solve[3] the axisymmetric thin-film equation [Eq. (5)] along with its boundary and initial conditions [Eqs. (6) and (7)] using a finite-difference scheme. We discretize the domain into an equidistant mesh of size $\Delta\tilde{r}$ using a second-order central differencing scheme for spatial discretization. Time discretization is performed using an implicit-explicit scheme of a constant time-step size $\Delta\tilde{t}$, wherein the fourth-order term describing capillary forces is discretized implicitly and the second-order term describing the nonlinear van der Waals forces is discretized explicitly. The mobility term ($\tilde{r}\tilde{h}^3$) is discretized as per the positivity-preserving scheme discussed in Diez *et al.* [34]. Based on our previous work [35], we use $\Delta\tilde{r} = 0.05$ and $\Delta\tilde{t} = \Delta\tilde{r}^{2.25}$, and confirm that the presented simulation results for lifetimes are grid and time-step size independent.

IV. RESULTS

A. Characterization of the film evolution for the governing parameter space

We start by characterizing the thinning dynamics for the governing parameter space. As explained, we fix μ, γ, A, and R_c such that the parameter space is spanned by the initial film thickness

[2]The above set of dimensionless governing equations [Eq. (5)] along with dimensionless initial and boundary conditions [Eqs. (7) and (6)] also apply to the case of surface bubbles, as long as we assume the bubble to approach a rigid surface that remains flat and the film to drain by capillary suction. To turn to the dimensional quantities, one should then use the following choices of scales: $h^* = h_o$, $r^* = \sqrt{h_o R_c/2}$, and $t^* = 3\mu R_c^2/\gamma h_o$.

[3]MATLAB files used for simulations available at github, doi: 10.5281/zenodo.3653037.

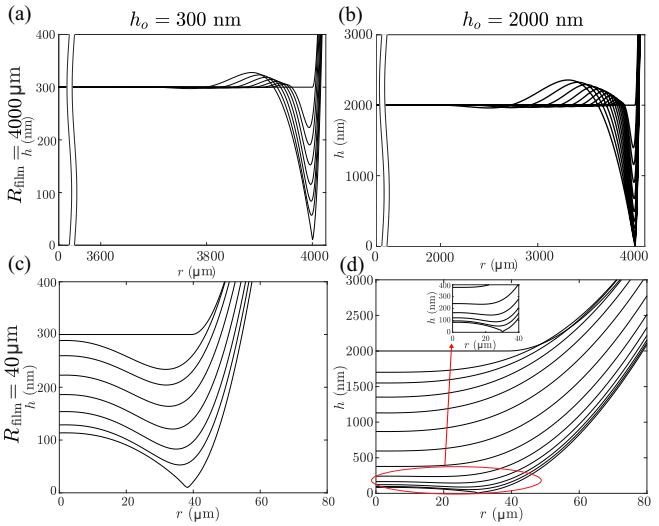

FIG. 3. Film evolution in space and time at the boundaries of our parameter space. Large films $R_{\text{film}} = 4000\ \mu$m of $h_0 = 300$ nm (a) and $h_o = 2000$ nm (b) initial thickness. The abscissa were made discontinuous to better illustrate the localized dimple for large film radius. Small films $R_{\text{film}} = 40\ \mu$m of $h_0 = 300$ nm (c) and $h_o = 2000$ nm (d) initial thickness. (c), (d) Film evolution in space and time for $R_{\text{film}} = 40\ \mu$m at $h_o = 300$ nm in (c) and $h_o = 2000$ nm in (d). Inset in (d): zoomed view of the film evolution at $t = t_r/2^n$ with $n = 5 \ldots 0$. Aside from the initial profiles at $t = 0$, profiles are shown for $t_r/2^n$, with $n = 6 \ldots 0$ in (a) and (c) and $n = 11 \ldots 0$ in (b) and (d), with $t_r = 22.87$, 150.48, 12.91, and 11.12 s for (a), (b), (c), and (d), respectively.

h_0 and film radius R_{film}. The lower limit of the film radius (40 μm) was chosen based on the experimentally observed values [25,36], while the upper limit (4000 μm) was chosen to approach the semi-infinite film asymptote [29,35,37]. The range of initial film thicknesses studied in this work is representative of the drainage experiments reported in the literature [7,36].

We start with a description of films with the largest radius ($R_{\text{film}} = 4000\ \mu$m) considered in this work, connecting their behavior to the well-known behavior of semi-infinite films [29,35,37]. The features of thinning of large films are the same for thin ($h_0 = 300$ nm) and thick ($h_0 = 2000$ nm) films. They are characterized by the formation of a local depression, called a dimple, near the connection between the flat and curved parts of the film, while the film at the center, i.e., at $r = 0$, remains unaffected [see Figs. 3(a) and 3(b)]. With the thinning being a localized phenomenon, the evolution of the film is insensitive to the film radius itself, given it is sufficiently large. Later in this paper, we quantitatively show that the large film radius limit considered in this work indeed approaches the behavior observed for semi-infinite films sometimes referred to as marginal pinching [29]. Having confirmed the behavior for such large films, we now continue with the focal point of the paper: the behavior of films with small radii.

The thinning behavior for the smallest film radius considered in this work ($R_{\text{film}} = 40\ \mu$m) is deliberately different from that for the largest films: film thinning initially occurs across the entire film as evident for thin and thick films in Figs. 3(c) and 3(d), respectively. Shortly prior to rupture, the films do develop a dimple. A prediction for the transition from uniform thinning to dimpled thinning was first developed by Joye *et al.* [7], who evaluated the ratio between the order of magnitude of the curvature at the center of the film $2h(t)/R_{\text{film}}^2$ and at the bubble $1/R_c$. Using numerical simulations, they found that films develop a dimple when this ratio decreases below a

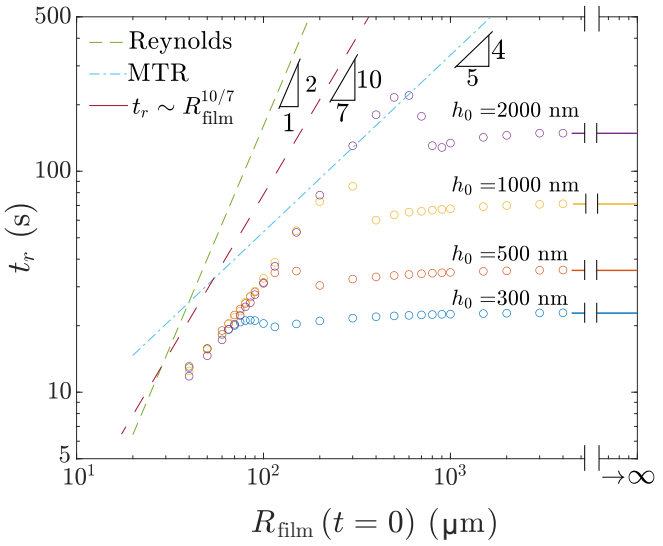

FIG. 4. Lifetime of the film as a function of the initial film radius, for different initial film thicknesses. Green and blue dashed lines correspond to the lifetimes calculated based on Reynolds' [1] and MTR theory [26], respectively. The red dashed line corresponds to lifetime calculated based on Eq. (19). The horizontal solid lines at the right of the figure signify the plateauing values of film lifetimes at large radius. These values are further used in Fig. 9 to compare with the mechanistic model developed for large films in Sec. IV D.

value of 0.7. For the here considered case with $R_c = 1.8$ mm and R_{film} at the time of rupture[4] being 38 and 30 μm for $h_o = 300$ and 2000 nm, respectively, Joye's criterion predicts a transition around $h(t) = 286$ and 175 nm, respectively, which is in good agreement with those found in Figs. 3(c) and 3(d).

B. Influence of initial film radius and film thickness on film lifetime

Having studied the film evolution at the boundaries of our parameter space, we now study how film lifetime depends on the initial film radius and film thickness. As anticipated, we observe two regimes with distinctly different behavior for small and large radii films as shown in Fig. 4.

For large radii films, the lifetime of a film is independent of the initial film radius and depends solely on the initial film thickness, confirming what is well established for semi-infinite films [37]. Briefly, the independence on film radius is explained by the thinning process being a localized phenomena, such that the radius of the film plays no role. Lifetimes are well described by our earlier developed model for semi-infinite two-dimensional (2D) films [37], after modification to account for the radial geometry considered in this work leading to $t_r \sim R_{\text{film}}^0 h_o^{5/7}$, as detailed in Sec. IV D.

For small radii films, film lifetime solely depends on the initial film radius and not on the initial film thickness, in qualitative agreement with the work by Malhotra and Wasan [23]. Our numerical data show t_r to scale with R_{film}^n, with the exponent $n = 1.1$ being smaller ($\approx$81%) than 2 from classical Reynolds' theory [1] and larger ($\approx$27%) than 4/5 from MTR theory [23,25]. The thin-film simulations as done in this work with h_o and R_{film} being direct input parameters hence clarify the

[4]The dimple does not necessarily remain at the location determined by the initial film radius during the film evolution. Once the interface relaxes from the discontinuous initial condition, the dimple initially moves toward the center, and then moves outward, with the final film radius at the instant of rupture in Figs. 3(c) and 3(d) being 38.34 and 30.22 μm, respectively, as compared to the initial film radius $R_{\text{film}} = 40$ μm.

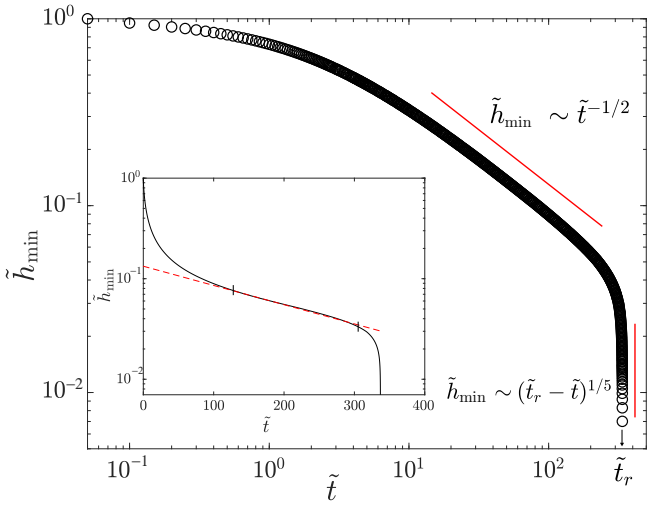

FIG. 5. Film dynamics for a prototypical small film ($R_{\text{film}} = 100$ μm), with initial thickness $h_o = 1000$ nm illustrating how the dimensionless minimum film thickness extracted from the numerical simulations evolves in time. The film evolution shows an early and a late stage, both governed by power-law dynamics (further detailed in Secs. IV C 1 and IV C 2). The inset shows the same data in a log-lin plot. The red dashed line shows an exponential fit from $0.03 < \tilde{h}_{\min}(t) < 0.08$ as used in Manev *et al.* [25]. When we recast the fitting parameters $\tilde{a}$ and $\tilde{b}$ to their dimensional equivalents we find these parameters as $a = 133$ nm and $b = 0.046$ Hz. While the value of a is not available to compare within the paper by Manev *et al.* [25], the value of b is within 15% of their experimentally determined values.

variety of different exponents reported in literature that were obtained under various simplifying assumptions. In order to develop a better understanding on key simplifying assumptions and provide mechanistic insights in the numerically obtained scaling relation between t_r, R_{film}, and h_o, we combine two known analytical solutions [6,30]. Full details on this model are provided in Sec. IV C. For the reader mainly interested in the outcome, the analytical description yields $t_r \sim h_o^0 R_{\text{film}}^{10/7}$, with the exponent for R_{film} in fair agreement ($\approx$30% larger) with the numerical data, as shown in Fig. 4. Although our mechanistic model does not give a better prediction than that provided by MTR theory, the strength of our model lies on the one hand in its simplicity, following directly from the thin-film formalism and, on the other hand, in its ability to capture the dynamics of dimple formation.

We close the discussion on Fig. 4 by briefly commenting on the observation that film lifetime does not monotonically reach the plateauing value observed for large radii film. We observe that the thinning behavior in the transition region is qualitatively different from that for the large radii films, with the dimple shifting to the center of the film and growing beyond the initial film thickness (see Appendix A, Fig. 10). Since the focal point of this paper has been to study small films, a deeper analysis of this behavior is beyond the scope of this study. We next discuss the analytical models used to explain the lifetimes of small and large radii films.

C. Mechanistic model for dynamics of films with small radius

In this section, we develop a mechanistic model that combines two known analytical solutions that were obtained for the early and late stage dynamics through simplifications of the thin-film equation. We start our analysis by (re)examining the two mechanisms in these two stages. In the early stage, thinning is primarily governed by capillary drainage, while van der Waals forces govern the late stage. These stages are clearly evident from a plot of the minimum film thickness as a function of time, as shown for a prototypical small film ($R_{\text{film}} = 100$ μm) in Fig. 5. Some previous works [12,13] captured the dynamics using a single exponential function, fitted to (and currently

found to describe) only a part of the evolution ($0.03 < \tilde{h}_{\min} < 0.08$) as shown in the inset of Fig. 5. Other works studied the early and late stages separately [6,29,30]. For films with small radius, films thin initially across the entire radius and later locally at the dimple [Figs. 3(c) and 3(d)]. Analytical models described for uniform and localized thinning due to van der Waals forces were developed by Frankel and Mysels [6] and Zhang and Lister [30], respectively, such that we have chosen their scaling rules for early and late stage dynamics. In Sec. IV C 3, we combine them to develop a theoretical model that describes how the lifetime of films depends on their initial features.

1. Scaling rule for the early stage

Frankel and Mysels [6] developed scaling rules for the evolution of the film thickness at the center h_c and at the minimum of the dimple $h_{\min}$. They arrived at these rules by first determining the shape of a dimple close to rupture based on a self-similar solution of Eqs. (1)–(4) after applying the following simplifying assumptions: (i) a quasisteady flow, (ii) $h_{\min} \ll h_c$ [5], (iii) negligible influence of van der Waals forces, (iv) inner far-field constant slope, and (v) outer far-field constant curvature. They then connect the dimple to the central part of the film by assuming it to be described by a parabola $h(r,t) = ar^2 + br + c$, and infer the dynamics of h_c and $h_{\min}$ by solving the continuity equation. On substituting the boundary conditions $h(r = 0, t) = h_c$, $\partial h/\partial r(r = 0, t) = 0$, and $h(r = R_{\text{film}}, t) = h_{\min}$ in the aforementioned parabola, along with the assumption of $h_{\min} \ll h_c$, results into a film profile $h(t) = h_c(1 - r^2/R_{\text{film}}^2)$. Using the two-dimensional flow rate $[Q = 1/(2\pi R_{\text{film}})d/dt(2\pi \int_0^{R_{\text{film}}} hr\,dr)]$ through the dimple, an inner far-field constant slope $-2h_c/R_{\text{film}}$ and a constant far-field outer curvature $2/R_c$, Frankel and Mysels [6] show[5] that h_c and $h_{\min}$ scale as

$$h_c = \left(\frac{3\mu R_{\text{film}}^6}{c_1 2^4 \gamma R_c t}\right)^{1/4} \tag{8}$$

and

$$h_{\min} = \frac{2c_1 c_2 h_c^2 R_c}{R_{\text{film}}^2}, \tag{9}$$

respectively. Here, $c_1 = 1.22$ and $c_2 = 1.25$ as determined by Frankel and Mysels [6] are the numerical solutions for the asymptotic curvature at the far-right boundary of the dimple and the minimum value of the film thickness at the dimple, respectively. On substituting for h_c from Eq. (8), in Eq. (9) we obtain

$$h_{\min} = \left(\frac{3\mu c_1 c_2^2 R_{\text{film}}^2 R_c}{2^4 \gamma t}\right)^{1/2}. \tag{10}$$

Nondimensionalizing Eq. (10), using $\tilde{R}_{\text{film}} = R_{\text{film}}/\sqrt{h_o R_c/4}$, $\tilde{t} = t/(3\mu R_c^2/2\gamma h_o)$, and $\tilde{h}_{\min} = h_{\min}/h_o$ as discussed in Sec. II, we obtain

$$\tilde{h}_{\min} = \left(\frac{c_1 c_2^2}{2^5}\frac{\tilde{R}_{\text{film}}^2}{\tilde{t}}\right)^{1/2}. \tag{11}$$

[5]The numerical factors in Eqs. (8) and (9) are adjusted to account for the difference in the definition of film thicknesses between our work (see Sec. II) and Frankel and Mysels [6]. More specifically, the constant 2^4 instead of 2^8 in Eq. (8) and the constant 2^0 instead of 2^1 in Eq. (9) stem from considering the upper half of an axisymmetric film between two bubbles in our work as compared to the full film thickness considered between the gas-liquid interface and the solid substrate in Frankel and Mysels [6].

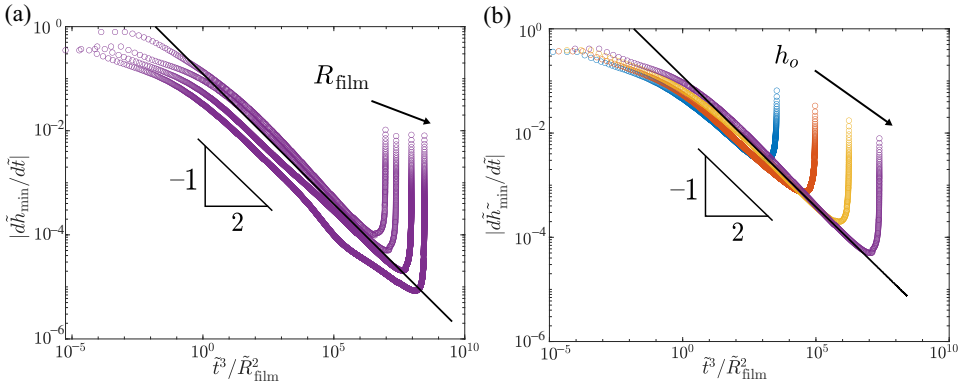

FIG. 6. Dimensionless thinning rate as a function of the rescaled time axis [based on Eq. (12)] illustrating early stage film dynamics for a fixed initial film thickness of $h_o = 2000$ nm and different $R_{\text{film}} = 50$, 100, 200, and 400 μm in (a); and for a fixed film radius of $R_{\text{film}} = 100$ μm and different $h_0 = 300$, 500, 1000, and 2000 nm in (b). The black solid lines correspond to Eq. (12).

We note that the starting point in the model derived by Frankel and Mysels [6] is the occurrence of a dimple, such that this equation holds near rupture. We hence expect this relation to describe the simulations, which start from a finite value of $\tilde{h}_{\min}$ at $\tilde{t} = 0$, after an initial transient. As commonly done in literature [7,24], rather than considering $\tilde{h}_{\min}$ in a comparison between theory and simulations, we compare the thinning rate

$$\frac{\partial \tilde{h}_{\min}}{\partial \tilde{t}} = -\frac{1}{2}\left(\frac{c_1 c_2^2}{2^5}\right)^{1/2}\left(\frac{\tilde{R}^2_{\text{film}}}{\tilde{t}^3}\right)^{1/2}. \tag{12}$$

This expression shows that the dimensionless thinning rate scales with time as $\tilde{t}^{-3/2}$, with film radius as $\tilde{R}^1_{\text{film}}$, and with film thickness as h_o^0. Comparing our simulations for different R_{film} and fixed h_o, we see a reasonable collapse of the curves when plotting the dimensionless rate against $\tilde{t}^3/\tilde{R}^2_{\text{film}}$ [Fig. 6(a)]. Furthermore, for different h_o and fixed $\tilde{R}_{\text{film}}$, we see that the early stage dynamics indeed does not depend on the initial film thickness [Fig. 6(b)].

As mentioned earlier, van der Waals forces are not included in the model by Frankel and Mysels [6]. Consequently, the film approaches rupture asymptotically, i.e., $\tilde{h}_{\min} = 0$ does not occur in a finite time. Thus, Eq. (12) on its own could not be used to predict the lifetime of the film. In the next section, we therefore consider the late stage governed by van der Waals forces separately.

2. Scaling rule for the late stage

Van der Waals forces induce a rapid rupture once the film is thinned sufficiently to a certain critical thickness h_{cr}. Considering the evolution of the dimple close to rupture where it is known to be independent of initial and boundary conditions [38], Zhang and Lister [30] developed a similarity solution for Eq. (1) to arrive at the following scaling:

$$\tilde{h}_{\min} = a_v\left(\frac{\tilde{t}_r - \tilde{t}}{144\kappa^2}\right)^{1/5}, \tag{13}$$

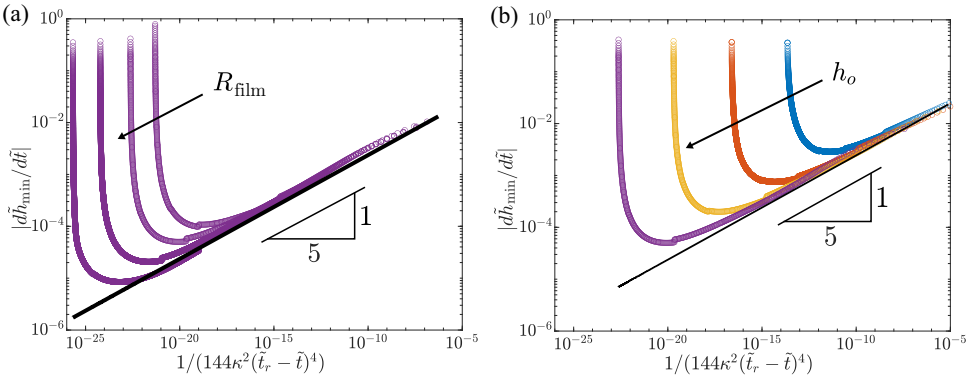

FIG. 7. Dimensionless thinning rate as a function of the rescaled time axis [based on Eq. (14)] illustrating late stage film dynamics for a fixed initial film thickness of $h_o = 2000$ nm and different $R_{\text{film}} = 50, 100, 200,$ and 400 μm in (a); and for a fixed film radius of $R_{\text{film}} = 100$ μm and different $h_0 = 300, 500, 1000,$ and 2000 nm in (b). The black solid lines correspond to Eq. (14).

where a_v is an $O(1)$ constant. Here, $144\kappa^2$ is a factor that relates $\tilde{t}_r$ and $\tilde{t}$ to a dimensionless time relevant for this late stage [30].[6] The thinning rate is then given by

$$\frac{\partial \tilde{h}_{\min}}{\partial \tilde{t}} = -\frac{a_v}{5}\left(\frac{1}{144\kappa^2(\tilde{t}_r - \tilde{t})^4}\right)^{1/5}. \tag{14}$$

Notably, the thinning rate in the late stage neither depends on the initial film thickness nor on the initial film radius. Replotting the data set shown in Figs. 6(a) and 6(b), now using the rescaled time axis $1/[144\kappa^2(\tilde{t}_r - \tilde{t})^4]$ all curves indeed collapse close to rupture as shown on the right-hand sides of Figs. 7(a) and 7(b).[7] The $O(1)$ constant is obtained by fitting the data to obtain $a_v = 1.18$.

3. Estimate of the film lifetime

To arrive at the total thinning rate, we consider the contribution of the early and the late stage [Eqs. (12) and (14)] as additive [37], to arrive at

$$\left(\frac{\partial \tilde{h}_{\min}}{\partial \tilde{t}}\right)_{\text{total}} = -\frac{1}{2}\left(\frac{c_1 c_2^2}{2^5}\right)^{1/2}\left(\frac{\tilde{R}_{\text{film}}^2}{\tilde{t}^3}\right)^{1/2} - \frac{a_v}{5}\left(\frac{1}{144\kappa^2(\tilde{t}_r - \tilde{t})^4}\right)^{1/5}. \tag{15}$$

On recasting $\tilde{t}$ and $(\tilde{t}_r - \tilde{t})$ in the first and the second terms on the right-hand side in terms of $\tilde{h}_{\min}$ using Eqs. (11) and (13), respectively, we obtain the total thinning rate as

$$\left(\frac{\partial \tilde{h}_{\min}}{\partial \tilde{t}}\right)_{\text{total}} = \left(\frac{-2^4}{c_1 c_2^2 \tilde{R}_{\text{film}}^2}\right)\tilde{h}_{\min}^3 - \frac{a_v^5}{720\tilde{h}_{\min}^4 \kappa^2}, \tag{16}$$

[6]Note that the ratio $(1/144\kappa^2)$ arises from the translation from the timescale based on the growth of unstable waves to the timescale based on drainage as used throughout this paper. More specifically, the length scale pertaining to the unstable waves is $h_o^2\sqrt{3\pi\gamma/A}$, which translates into a timescale $216\pi^2\gamma\mu h_o^5/A^2$.

[7]We note that the nonsmooth connection between the early and late stage arises from a shift in the location of the dimple (as for instance seen in Fig. 3). In our simulations, this shift occurs by one grid point such that it appears as a noncontinuous jump.

which is independent of time. An estimate for the lifetime can then be obtained as

$$\tilde{t}_r = \int_0^{\tilde{t}_r} \partial\tilde{t} = \int_1^0 \frac{\partial\tilde{h}_{\min}}{\left(\frac{-2^4}{c_1 c_2^2 \tilde{R}_{\text{film}}^2}\right)\tilde{h}_{\min}^3 - \frac{a_v^5}{720\tilde{h}_{\min}^4\kappa^2}}. \tag{17}$$

The solution of the above integral[8] at the limit $\tilde{R}_{\text{film}} \to 0$, for any value of κ, gives

$$\tilde{t}_r = 0.65\,\tilde{R}_{\text{film}}^{10/7}\kappa^{4/7}, \tag{18}$$

On substituting back the relevant length and timescales from Sec. II, we get

$$t_r = 0.65\left(\frac{R_{\text{film}}}{r^*}\right)^{10/7}\left(\frac{\pi h_o^3\gamma}{AR_c}\right)^{4/7} t^* = 5.05 R_{\text{film}}^{10/7}\gamma^{-3/7}A^{-4/7}R_c^{5/7}. \tag{19}$$

This analysis shows that the dimensional lifetime is independent of the initial thickness h_o and scales with the radius R_{film} with an exponent of 10/7. This result is plotted in Fig. 4 as the dashed red line. Given the simplifying assumptions used to derive the similarity solutions for the early and late stage, Eq. (19) fairly well describes the numerical data, as shown in Fig. 4. We note that the timescale of the early stage is much larger than that of the late stage, such that an alternative way to determine the total lifetime is to solely consider the early stage and determine the time it takes to reach a critical thickness for which different empirical correlations are available in the literature [2,22,24,39]. The strength of the here presented analytical model is that it does not require empirical correlations. In fact, the model allows to determine a theoretical prediction of the critical thickness. We end this section by demonstrating that we can obtain an estimate of critical film thickness by following the approach developed by Vrij [2]. Vrij [2] proposed that the crossover from the early stage to the late stage occurs via an inflection point, wherein both the film thickness and its first derivative need to be continuous and identical. Equating film thicknesses for the two stages as described in Eqs. (11) and (13), and the derivatives of the film thicknesses as described in Eqs. (12) and (14), gives the time $\tilde{t}_{cr} = 0.55\tilde{R}_{\text{film}}^{10/7}\kappa^{4/7}$ at which the crossover happens from the early stage to the late stage. Substituting this estimate of $\tilde{t}_{cr}$ in Eq. (11), we obtain an estimate of the critical film thickness $\tilde{h}_{cr} = 0.33(\tilde{R}_{\text{film}}/\kappa)^{2/7}$, which on substituting the scales yield $h_{cr} = 0.29(R_{\text{film}}^2 R_c A^2/\gamma^2)^{1/7}$. Depending on the correlations used to relate the film thinning velocity with the film radius, the exponent for the film radius in $h_{cr} \sim R_{\text{film}}^x$ obtained in the literature is in the range 0.11–0.48 [22,24,39]. Our exponent of 2/7 is in agreement with that found by Vrij [2].

D. Mechanistic model for dynamics of films with large radius

In this section, we adapt our earlier model developed for semi-infinite films in a 2D Cartesian geometry to the axisymmetric geometry considered in this paper. Film thinning for these films is observed to proceed via the formation of a localized dimple at the edge of the film, as shown in Figs. 3(a) and 3(b). Aradian *et al.* [29] extended the model developed by Frankel and Mysels [6] to account for localized dimpling observed for large films. We therefore begin the model description by studying the early stage dynamics that follows the scaling rule developed by Aradian *et al.* [29]:

$$\tilde{h}_{\min} = a_r\tilde{t}^{-1/2}, \tag{20}$$

which on taking the time derivative leads to

$$\frac{\partial\tilde{h}_{\min}}{\partial\tilde{t}} = -\frac{a_r}{2\tilde{t}^{3/2}}. \tag{21}$$

[8]The exact solution is an impractically long solution and hence we solve it at limit $R_{\text{film}} \to 0$ and $R_{\text{film}} \to \infty$ to arrive at an approximate, but compact solution. The relative difference between the actual solution and the approximate solution (18) is approximately 1%.

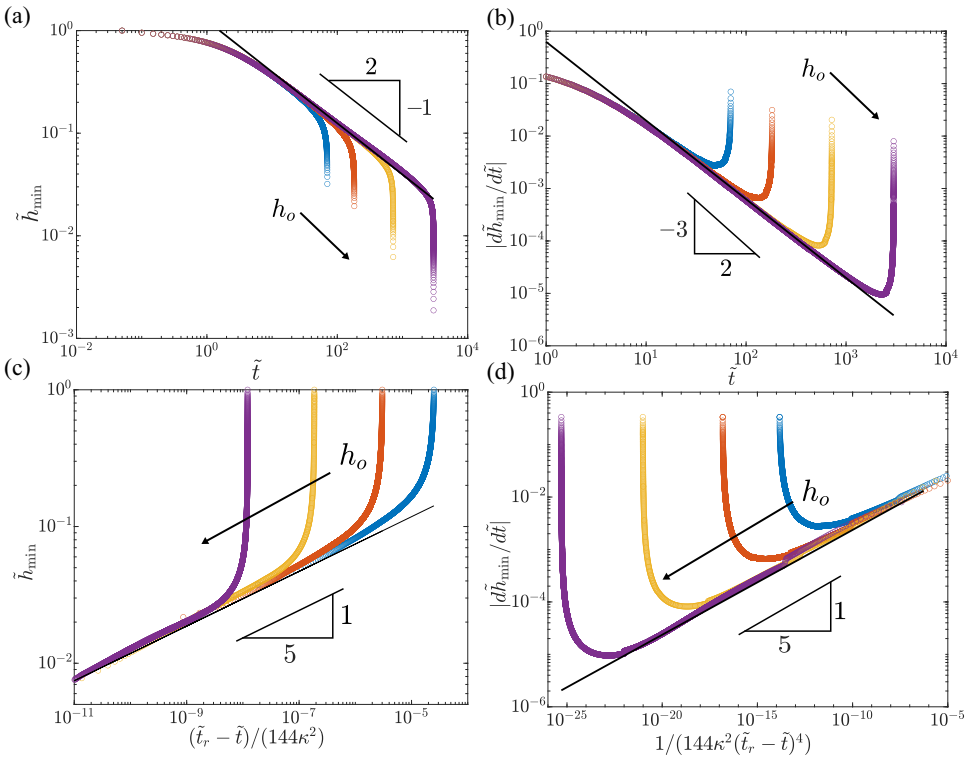

FIG. 8. Dimensionless film thickness and thinning rate as a function of time illustrating the early stage in (a) and (b), respectively, and the late stage film dynamics in (c) and (d), respectively, for a fixed film radius of $R_{\text{film}} = 4000\ \mu$m and different initial film thicknesses of $h_o = 300$, 500, 1000, and 2000 nm. The black solid lines in (a), (b), (c), and (d) correspond to Eqs. (20), (21), (13), and (14), respectively.

Figures 8(a) and 8(b) show how the early stage film dynamics from numerical simulations for these large films compare for different initial film thicknesses for a fixed large $R_{\text{film}} = 4000\ \mu$m. The data are well described by the model, after a first initial transient. The $O(1)$ constant obtained from a fit of the data is $a_r = 1.2$. To confirm that the scaling in Eq. (21) is independent of R_{film}, we also analyzed the early stage dynamics for $R_{\text{film}} = 1000$, 2000, and 4000 μm. We confirm that those are well described by Eq. (21) (model by Aradian *et al.* [29]), but not by Eq. (12) (model by Frankel and Mysels [6]) (see Appendix B, Fig. 11).

The late stage evolution for these large axisymmetric films follows the model by Zhang and Lister [30] presented in Eqs. (13) and (14), with the earlier reported $O(1)$ constant $a_v = 1.18$. Figures 8(c) and 8(d) show how our numerical simulations follow the late stage dynamics for different h_o and for $R_{\text{film}} = 4000\ \mu$m.

Considering the contribution of the early and the late stages as additive and using the same approach as presented in the main body of the paper, we arrive at the total thinning rate

$$\left(\frac{\partial \tilde{h}_{\min}}{\partial \tilde{t}}\right)_{\text{total}} = -\frac{a_r}{2\tilde{t}^{3/2}} - \frac{a_v}{5}\left(\frac{1}{144\kappa^2(\tilde{t}_r - \tilde{t})^4}\right)^{1/5}, \tag{22}$$

which, when represented in terms of $\tilde{h}_{\min}$, reads as

$$\left(\frac{\partial \tilde{h}_{\min}}{\partial \tilde{t}}\right)_{\text{total}} = -\frac{\tilde{h}_{\min}^3}{2a_r^2} - \frac{a_v^5}{720\tilde{h}_{\min}^4\kappa^2}. \tag{23}$$

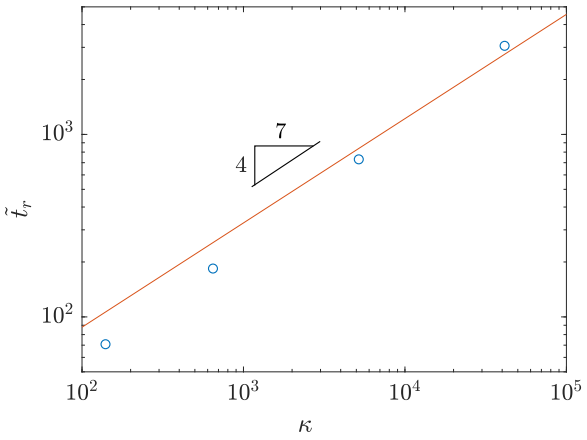

FIG. 9. Dimensionless film rupture times as a function of dimensionless curvature for the large film asymptotes at the extreme right in Fig. 4. The blue circles correspond to the numerical simulations whereas the red line corresponds to the theoretical expression as described in Eq. (25).

An estimate for the film rupture time can then be obtained as

$$\tilde{t}_r = \int_0^{\tilde{t}_r} \partial\tilde{t} = -\int_1^0 \frac{\partial\tilde{h}_{\min}}{\frac{\tilde{h}_{\min}^3}{2a_r^2} + \frac{a_v^5}{720\tilde{h}_{\min}^4\kappa^2}}. \tag{24}$$

The solution of the above integral at the limit $\kappa \to \infty$ gives

$$\tilde{t}_r = 6.32\kappa^{4/7}. \tag{25}$$

Figure 9 shows how large film asymptotes from Fig. 4 agree well with the theoretical model (25). On substituting the scales in Eq. (25) to determine the dimensional lifetime, we obtain

$$t_r = 18.2\mu R_c^{10/7}\gamma^{-3/7}A^{-4/7}h_o^{5/7}R_{\text{film}}^0. \tag{26}$$

For large film radii, we hence find that the dimensional lifetime of the film depends on the initial film thickness and is independent of the film radius.

V. CONCLUSIONS

The aim of this work is to understand how the thinning dynamics and lifetime of films between two bubbles depend on the extent to which the bubbles have deformed upon close contact, as characterized by the initial radius and thickness of the flattened film. Numerical solutions of a hydrodynamic thin-film model show that the thinning dynamics are distinctly different for films of large and small initial radius. Large films thin locally through the formation of a dimple at the edge of the film [29], while small films initially thin across the entire film, then develop a dimple, and eventually rupture at the minimum of this dimple. For large films, our simulations confirm earlier theoretical work on films of semi-infinite radius [37] that predicts that the lifetime t_r scales with initial film radius R_{film} and thickness h_0 as $t_r \sim R_{\text{film}}^0 h_0^{5/7}$. As opposed to this scaling for large films, we found the lifetime of small films, which was the focus of this work, to be independent of the initial film thickness and dependent on film radius. To understand the scaling for small films, we combined earlier-reported analytical solutions for dimpled thinning in the early stage [6] and van der Waals rupture in the late stage [30]. While these analytical solutions were obtained through simplification of the full thin-film equation, the predicted scaling $t_r \sim h_0 R_{\text{film}}^{10/7}$ captures the trend in the numerical data reasonably well.

ACKNOWLEDGMENT

This work is supported by the Netherlands Organization for Scientific Research (NWO) and the Dutch Institute for Sustainable Process Technology (ISPT) as part of the project COFILM.

APPENDIX A: FILM EVOLUTION AT THE TRANSITION REGION

The thinning behavior at the transition region is illustrated for a thin ($h_o = 300$ nm) and thick ($h_o = 2000$ nm) film in Fig. 10, for which the transition occurs around $R_{\text{film}} = 80$ and 600 μm, respectively. As expected, the film thinning is observed to proceed via the formation of a dimple at the connection between the planar and the curved portion of the film. Qualitatively, the difference in the film thinning at this transition region from that at the large radii films is that the film thickness at the center of the film increases beyond the initial film thickness. The physics behind film dynamics for films in this transition region is beyond the scope of this work.

APPENDIX B: THINNING DYNAMICS FOR LARGE FILMS: DEPENDENCE ON R_{film}

Figure 11 shows thinning rates for large film radii films and how they compare with the thinning rates obtained using the self-similar solutions of Frankel and Mysels [6] and Aradian *et al.* [29]. We find that our numerical data show a significant deviation with the self-similar solution by Frankel and Mysels [6], whereas it shows a reasonable fit the self-similar solution by Aradian *et al.* [29]. This further emphasizes that the thinning dynamics for large films is independent of the film radius and forms a strong basis to choose the self-similar solution by Aradian *et al.* [29] to explain the early stage dynamics for such films.

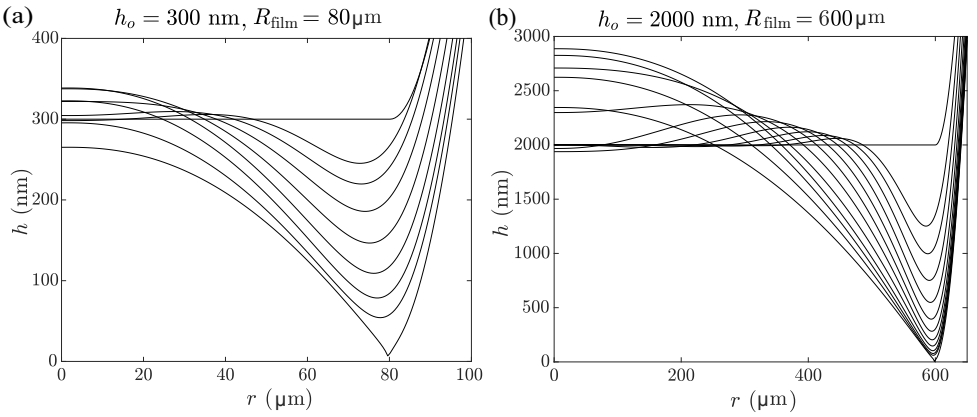

FIG. 10. Film evolution in the transition regime for two examples: (a) a thin film ($h_0 = 300$ nm), which has the transition around $R_{\text{film}} = 80$ μm, and (b) a thick film ($h_0 = 2000$ nm), with the transition around $R_{\text{film}} = 600$ μm. Aside from the initial profiles at $t = 0$, profiles are shown for $t_r/2^n$, with $n = 7 \ldots 0$ in (a) and $n = 11 \ldots 0$ in (b), with $t_r = 11.0$ s and 220.4 s for (a) and (b), respectively.

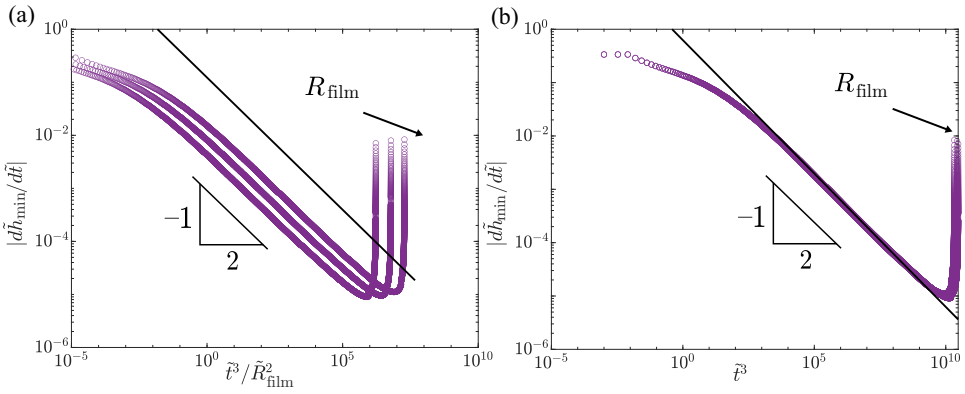

FIG. 11. Dimensionless thinning rate as a function of the rescaled time axis based on Eq. (12) (shown using black solid line) in (a) and based on Eq. (21) (shown using black solid line) in (b) illustrating early stage film dynamics for a fixed initial film thickness of $h_o = 2000$ nm and different $R_{\text{film}} = 1000,\ 2000$, and 4000 μm.

[1] O. Reynolds, On the theory of lubrication and its application to Mr. Beauchamp tower's experiments, including an experimental determination of the viscosity of olive oil, Philos. Trans. R. Soc. London **177**, 157 (1886).

[2] A. Vrij, Possible mechanism for the spontaneous rupture of thin, free liquid films, Discuss. Faraday Soc. **42**, 23 (1966).

[3] P. S. Prokhorov, The effects of humidity deficit on coagulation processes and the coalescence of liquid drops, Discuss. Faraday Soc. **18**, 41 (1954).

[4] R. S. Allan, G. E. Charles, and S. G. Mason, The approach of gas bubbles to a gas/liquid interface, J. Colloid Sci. **16**, 150 (1961).

[5] D. Platikanov, Experimental investigation on the "dimpling" of thin liquid films, J. Phys. Chem. **68**, 3619 (1964).

[6] S. P. Frankel and K. J. Mysels, On the "dimpling" during the approach of two interfaces, J. Phys. Chem. **66**, 190 (1962).

[7] J. L. Joye, G. J. Hirasaki, and C. A. Miller, Dimple formation and behavior during axisymmetrical foam film drainage, Langmuir **8**, 3083 (1992).

[8] G. Singh, C. A. Miller, and G. J. Hirasaki, On dimple formation in foam films, J. Colloid Interface Sci. **187**, 334 (1997).

[9] I. U. Vakarelski, R. Manica, X. Tang, S. J. O-Shea, G. W. Stevens, F. Grieser, R. R. Dagastine, and D. Y. C. Chan, Dynamic interactions between microbubbles in water, Proc. Natl. Acad. Sci. USA **107**, 11177 (2010).

[10] B. Liu, R. Manica, Q. Liu, E. Klaseboer, Z. Xu, and G. Xie, Coalescence of Bubbles with Mobile Interfaces in Water, Phys. Rev. Lett. **122**, 194501 (2019).

[11] E. Klaseboer, J. Ph. Chevaillier, C. Gourdon, and O. Masbernat, Film drainage between colliding drops at constant approach velocity: Experiments and modeling, J. Colloid Interface Sci. **229**, 274 (2000).

[12] R. Manica, E. Klaseboer, and D. Y. C. Chan, Dynamic interactions between drops–a critical assessment, Soft Matter **4**, 1613 (2008).

[13] L. R. Fisher, D. Hewitt, E. E. Mitchell, J. Ralston, and J. Wolfe, The drainage of an aqueous film between a solid plane and an air bubble, Adv. Colloid Interface Sci. **39**, 397 (1992).

[14] R. Manica, L. Parkinson, J. Ralston, and D. Y. C. Chan, Interpreting the dynamic interaction between a very small rising bubble and a hydrophilic titania surface, J. Phys. Chem. C **114**, 1942 (2010).

[15] R. F. Tabor, R. Manica, D. Y. C. Chan, F. Grieser, and R. R. Dagastine, Repulsive Van Der Waals Forces in Soft Matter: Why Bubbles Do Not Stick to Walls, Phys. Rev. Lett. **106**, 064501 (2011).
[16] J. N. Connor and R. G. Horn, The influence of surface forces on thin film drainage between a fluid drop and a flat solid, Faraday Discuss. **123**, 193 (2003).
[17] R. Manica, J. N. Connor, L. Y. Clasohm, S. L. Carnie, R. G. Horn, and D. Y. C. Chan, Transient responses of a wetting film to mechanical and electrical perturbations, Langmuir **24**, 1381 (2008).
[18] D. Exerowa and P. M. Kruglyakov, *Foam and Foam Films: Theory, Experiment, Application* (Elsevier, Amsterdam, 1997).
[19] D. Y. C. Chan, E. Klaseboer, and R. Manica, Film drainage and coalescence between deformable drops and bubbles, Soft Matter **7**, 2235 (2011).
[20] R. K. Prud'homme, *Foams: Theory, Measurements, and Applications* (Routledge, Abingdon, UK, 2017).
[21] D. S. Dimitrov and I. B. Ivanov, Hydrodynamics of thin liquid films. on the rate of thinning of microscopic films with deformable interfaces, J. Colloid Interface Sci. **64**, 97 (1978).
[22] A. Sharma and E. Ruckenstein, Stability, critical thickness, and the time of rupture of thinning foam and emulsion films, Langmuir **3**, 760 (1987).
[23] A. K. Malhotra and D. T. Wasan, Effect of film size on drainage of foam and emulsion films, AIChE J. **33**, 1533 (1987).
[24] B. P. Radoev, A. D. Scheludko, and E. D. Manev, Critical thickness of thin liquid films: Theory and experiment, J. Colloid Interface Sci. **95**, 254 (1983).
[25] E. Manev, R. Tsekov, and B. Radoev, Effect of thickness non-homogeneity on the kinetic behavior of microscopic foam film, J. Dispersion Sci. Technol. **18**, 769 (1997).
[26] R. Tsekov, The r4/5-problem in the drainage of dimpled thin liquid films, Colloids Surf. A **141**, 161 (1998).
[27] E. Ruckenstein and A. Sharma., A new mechanism of film thinning: Enhancement of Reynolds' velocity by surface waves, J. Colloid Interface Sci. **119**, 1 (1987).
[28] A. N. Zdravkov, G. W. M Peters, and H. E. H. Meijer, Film drainage between two captive drops: Peo-water in silicon oil, J. Colloid Interface Sci. **266**, 195 (2003).
[29] A. Aradian, E. Raphael, and P. G. de Gennes, Marginal pinching in soap films, Europhys. Lett. **55**, 834 (2001).
[30] W. W. Zhang and J. R. Lister, Similarity solutions for van der waals rupture of a thin film on a solid substrate, Phys. Fluids **11**, 2454 (1999).
[31] A. Oron, S. H. Davis, and S. G. Bankoff, Long-scale evolution of thin liquid films, Rev. Mod. Phys. **69**, 931 (1997).
[32] G. K. Batchelor, *An Introduction to Fluid Dynamics*, Cambridge Mathematical Library (Cambridge University Press, Cambridge, 2000).
[33] See Supplemental Material at http://link.aps.org/supplemental/10.1103/PhysRevFluids.6.013603 for details on the derivation of the initial condition with a transition region.
[34] J. A. Diez, L. Kondic, and A. Bertozzi, Global models for moving contact lines, Phys. Rev. E **63**, 011208 (2000).
[35] M. S. Shah, V. van Steijn, C. R. Kleijn, and M. T. Kreutzer, Thermal fluctuations in capillary thinning of thin liquid films, J. Fluid Mech. **876**, 1090 (2019).
[36] E. D. Manev, S. V. Sazdanova, and D. T. Wasan, Emulsion and foam stability–the effect of film size on film drainage, J. Colloid Interface Sci. **97**, 591 (1984).
[37] M. T. Kreutzer, M. S. Shah, P. Parthiban, and S. A. Khan, Evolution of nonconformal landau-levich-bretherton films of partially wetting liquids, Phys. Rev. Fluids **3**, 014203 (2018).
[38] L. G. Leal, *Advanced Transport Phenomena: Fluid Mechanics and Convective Transport Processes* (Cambridge University Press, Cambridge, 2007).
[39] J. E. Coons, P. J. Halley, S. A. McGlashan, and T. Tran-Cong, A review of drainage and spontaneous rupture in free standing thin films with tangentially immobile interfaces, Adv. Colloid Interface Sci. **105**, 3 (2003).